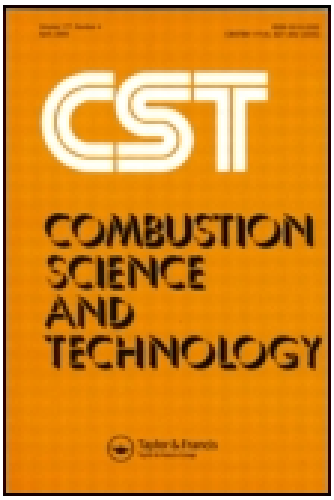

Combustion Science and Technology
Publication details, including instructions for authors and subscription information:
http://www.tandfonline.com/loi/gcst20

Experimental Study on the Combustion and NOx Emission Characteristics of DME/LPG Blended Fuel Using Counterflow Burner

Dongjo Lee [a], Jae Seong Lee [b], Ho Young Kim [b], Chul Kyun Chun [c], Scott C. James [d] & Sam S. Yoon [b]

[a] Technical Research Laboratories, POSCO, Pohang, Korea

[b] School of Mechanical Engineering, Korea University, Seoul, Korea

[c] Department of Mechanical Engineering, Mokpo National University, Mokpo, Korea

[d] Thermal/Fluid Science & Engineering, Sandia National Laboratories, Livermore, California, USA

Published online: 22 Dec 2011.

To cite this article: Dongjo Lee, Jae Seong Lee, Ho Young Kim, Chul Kyun Chun, Scott C. James & Sam S. Yoon (2012) Experimental Study on the Combustion and NOx Emission Characteristics of DME/LPG Blended Fuel Using Counterflow Burner, Combustion Science and Technology, 184:1, 97-113, DOI: 10.1080/00102202.2011.622319

To link to this article: http://dx.doi.org/10.1080/00102202.2011.622319

Combust. Sci. Technol., 184: 97–113, 2012

ISSN: 0010-2202 print/1563-521X online
DOI: 10.1080/00102202.2011.622319

Taylor & Francis
Taylor & Francis Group

EXPERIMENTAL STUDY ON THE COMBUSTION AND NOx EMISSION CHARACTERISTICS OF DME/LPG BLENDED FUEL USING COUNTERFLOW BURNER

Dongjo Lee,[1] Jae Seong Lee,[2] Ho Young Kim,[2] Chul Kyun Chun,[3] Scott C. James,[4] and Sam S. Yoon[2]

[1]*Technical Research Laboratories, POSCO, Pohang, Korea*
[2]*School of Mechanical Engineering, Korea University, Seoul, Korea*
[3]*Department of Mechanical Engineering, Mokpo National University, Mokpo, Korea*
[4]*Thermal/Fluid Science & Engineering, Sandia National Laboratories, Livermore, California, USA*

Dimethyl ether (DME) continues to be considered as an alternative fuel to conventional hydrocarbon fuels. Specifically, DME has been considered as a substitute fuel for liquefied petroleum gas (LPG) because the physical and chemical characteristics of DME are similar to those of LPG. However, the combustion performance for DME has not yet been established. In this study, the combustion and NOx-emission characteristics of LPG, DME, and an LPG/DME-blended fuel were experimentally investigated in a counterflow nonpremixed flame. The flame structure, flame temperature, NOx concentration, and distribution of OH radicals are reported. In this experimental study, the types of LPG used were butane 100%, butane 80% + propane 20%, and butane 75% + propane 25% by mass with DME mole fraction varied from 0 to 100 mole%. The experimental results indicated that the combustion and NOx emission characteristics of LPG fuels varied with the DME mole fraction. As the DME mole fraction increased, the flame thickness increased, but the flame length decreased. Also, the flame became wider, and its origin moved closer to the oxidizer nozzle with increasing DME mole fraction. In addition, as the DME mole fraction increased, the maximum flame temperature increased due to fast pyrolysis of DME as a result of the high oxygen content (~35% by mass) in DME. Moreover, NOx concentration decreased with increasing DME mole fraction in all LPGs.

Keywords: Counterflow burner; Distribution of OH radicals; DME/LPG blended fuel; Nonpremixed flame; NOx emission

INTRODUCTION

In the mid-19th century, petroleum was abundant, so it accommodated most of the energy needs of our society and propelled the industrial revolution. However, the world energy demand of modern times has increased dramatically, largely due to the

Received 23 November 2010; revised 23 August 2011; accepted 7 September 2011.
Address correspondence to Ho Young Kim, School of Mechanical Engineering, Korea University, Anamdong, 5-Ga, Sungbukgu, Seoul 136-701, Korea. E-mail: kimhy@korea.ac.kr

energy requirements of developing nations. Simultaneously, conventional fossil fuel supplies have notably decreased as reserves are exhausted. Also, air pollution has become the most serious global environmental problem, requiring cleaner alternative fuels. One means of reducing the dependency on petroleum products is to use fuels derived from natural gas, biomass, or coal. The use of oxygenated hydrocarbons, such as alcohols and ethers, as substitutes for petroleum-driven fuels has been extensively investigated in recent years. Oxygenates are attractive fuels and fuel additives in a broad range of combustion applications because of their clean burning characteristics, which lead to reduced emissions of carbon monoxide, reactive hydrocarbons, and nitrogen oxides (Arcoumanus et al., 2008; Semelsberger et al., 2006; Zhang et al., 2006).

The physical properties of dimethyl ether (DME) and liquefied petroleum gas (LPG) are quite similar, as shown in Table 1. Thus, existing land- and ocean-based LPG infrastructures can be used to manage DME, requiring minor modifications to the seals and gaskets (Lee, Seo et al., 2009; Marchionna et al., 2008; Ohno et al., 2000). In addition, DME generates less soot and unburned hydrocarbons in exhaust gases because of fast fuel/air mixing due to its relatively low boiling point (−25.1°C), absence of direct carbon-to-carbon bond, and high oxygen content (~35% by mass) (Morsy and Chung, 2007; Song et al., 2003; Ying et al., 2006; Yoon et al., 2008).

Because the physical and chemical characteristics of DME are so similar to those of LPG, DME has been specifically identified as substitute fuel for LPG. Due to the ever increasing price of LPG, DME and LPG/DME blended fuel have been widely suggested as alternatives or additives for use in cooking, heating, and LPG-fueled vehicles. Moreover, the LPG/DME-blended fuel would be the simplest way for quick penetration of DME into the fuel market.

The use of the DME/LPG-blended fuel in a conventional LPG-fueled system was previously studied. Marchionna et al. (2008) demonstrated the potential of DME as a substitute fuel in LPG-fueled domestic appliances. They performed combustion tests of LPG-fueled ovens using propane and butane with various concentrations of added DME added. They showed that a mixture of DME/LPG (DME: 15–20

Table 1 Fuel properties

Properties	DME	Propane	n-Butane
Chemical formula	CH_3OCH_3	C_3H_8	C_4H_{10}
Boiling point [°C/K]	−25.1/248.1	−42/231	−0.5/272.7
Liquid density [g/cm^3]	0.67	0.49	0.57
Specific gravity (vs. air)	1.59	1.52	2.01
Vapor pressure at 0°C [atm]	6.1	9.3	2.4
Flammability limits in air [vol. %]	3.4–17	2.1–9.4	1.9–8.4
Ignition temperature [°C/K]	235/508	470/743	365/638
Max. burning velocity [cm/s]	50	43	43
Stoichiometric air/fuel ratio [kg/kg]	9.0	15.7	15.5
Lower heating value [MJ/kg]	28.8	46.3	45.7
Molecular weight	46.07	44.11	58.12
Adiabatic flame temp. [K]	2227	2250	2240
Cetane number	55–60	(5)	(10)
Liquid viscosity at 25°C (kg/ms)	0.15	0.21	0.32

vol.%) yielded significant improvements over pure DME without the need for system modification. Lee, Oh et al. (2009) experimentally studied whether a DME/LPG-blended fuel would be acceptable in spark-ignition engines. According to their research, DME is a clean and efficient fuel for spark-ignition engines for ~20% DME by mass in LPG. Engine power was comparable to that of pure LPG for up to 10% DME by mass; however, engine power output decreased with higher percentages of DME because the energy content of DME is notably lower than that of LPG (see Table 1). Also, engine knock increased with higher mass percentage of DME because of its high cetane number.

Most research on DME has focused on engine applications, and only a few studies exist that have explored the fundamental combustion characteristics of DME and DME/LPG-blended fuels in variable content ratios. These fundamental studies (using a counterflow diffusion flame) should be completed prior to DME use in complex engines, combustors, or burners. The safety and efficiency of using DME as a substitute or additive to LPG has not been fully established. To use DME in a wide range of applications, more data on the combustion and emission characteristics of LPG/DME-blended fuels are required.

In this study, the combustion and NOx emission characteristics of LPG, DME, and an LPG/DME-blended fuel are experimentally investigated using a counterflow nonpremixed flame. Photos of the flame structures are taken with direct and Schlieren photography, flame temperatures were collected with an R-type thermocouple, NOx concentrations were measured with chemiluminescence, and distribution of OH radicals was described with OH-planar-laser-induced fluorescence (PLIF). Reliable data for LPG/DME-blended fuels are compiled.

EXPERIMENTAL APPARATUS AND METHOD

In this study, as shown in Table 2, LPG and DME ratios varied from butane 100% (mass) to butane 75% + propane 25% (mass) and from 0 to 100 mole%, respectively.

Laminar counterflow diffusion flames provide useful information concerning the basic characteristics of nonpremixed combustion. Figure 1 shows the experimental

Table 2 Fuel supply conditions for DME/LPG mixtures

Type			Mole/weight fraction								
A	LPG	mole %	100	97	95	93	90	70	50	25	0
	DME	mole %	0	3	5	7	10	30	50	75	100
		mass %	0	2.4	4.0	5.6	8.1	25.4	44.2	70.4	100
B	LPG	mole %	100	97	95	93	90	70	50	25	0
	DME	mole %	0	3	5	7	10	30	50	75	100
		mass %	0	2.5	4.2	5.9	8.5	26.3	45.5	71.4	100
C	LPG	mole %	100	97	95	93	90	70	50	25	0
	DME	mole %	0	3	5	7	10	30	50	75	100
		mass %	0	2.5	4.3	6	8.6	26.5	45.8	71.7	100

Type A: Butane 100% + Propane 0% (mass).
Type B: Butane 80% + Propane 20% (mass).
Type C: Butane 75% + Propane 25% (mass).

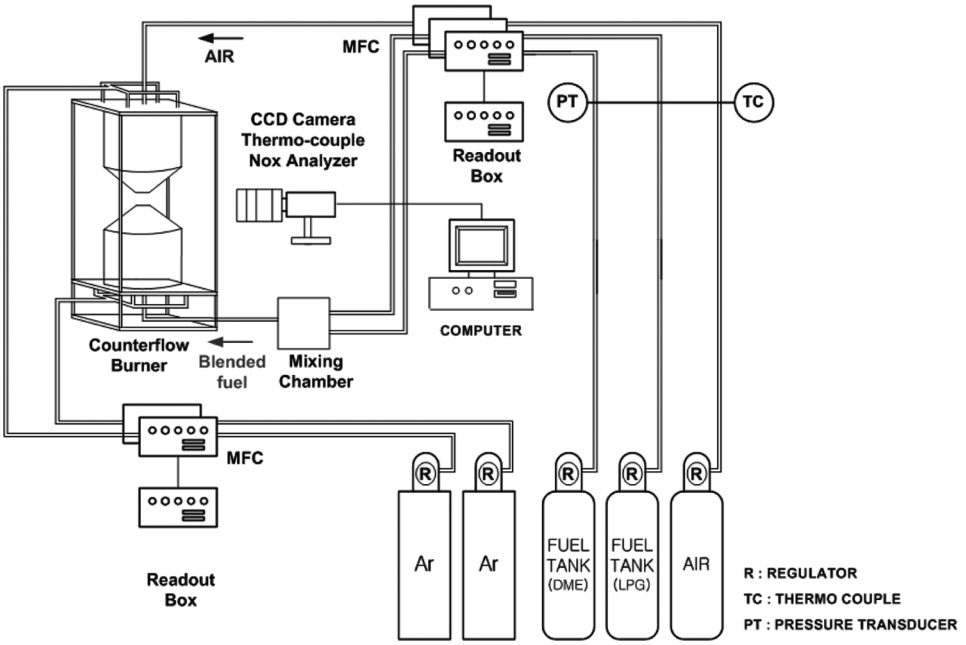

Figure 1 Schematic of the experimental apparatus.

apparatus consisting of four parts: a burner, a mixing chamber, a flow controller, and a system for data collection. The burner has counterflowing jets composed of two identical, vertically aligned cylindrical burners with inner diameter of 10 mm and outer diameter of 20 mm. The distance between the burners was maintained at $L = 10$ mm. Each nozzle was surrounded by a coaxial nozzle issuing argon to stabilize the flame. As shown in Figure 2a, each burner has a 25:1 contraction and contains a series of small wire-mesh screens, 1-mm glass beads, and honeycombs to produce a uniform velocity profile at the exit plane. Air (oxidizer), argon (shield), LPG, and DME fuel were independently regulated by a set of digital mass flow controllers (MFC; Brooks 5850E), which deliver gas within 0.5% accuracy for the full operating range.

As shown in Figures 2b and 2c, a counterflow diffusion flame was established between gases coming out of the upper and lower burners; the LPG, DME, or LPG/DME-blended fuel was introduced through the lower burner and high-purity (99.99%) air comprising 20.9% oxygen and 79.1% nitrogen issued from the upper burner at 1000 standard cubic centimeters per minute (sccm). A 2-L, glass-bead-filled mixing chamber was used to blend the LPG and DME fuels.

Figure 2c shows photos of a pure-butane diffusion flame with an illuminated stagnation plane. The experimental conditions and parameters are listed in Table 3. The stagnation plane was observed by offsetting an additional light source in a different direction than the main light source.

Figure 3 shows the experimental setup of the planar laser induced fluorescence (PLIF) system for measuring the distribution of OH radicals. The standard laser arrangement for OH LIF detection was used in our experiments. The second

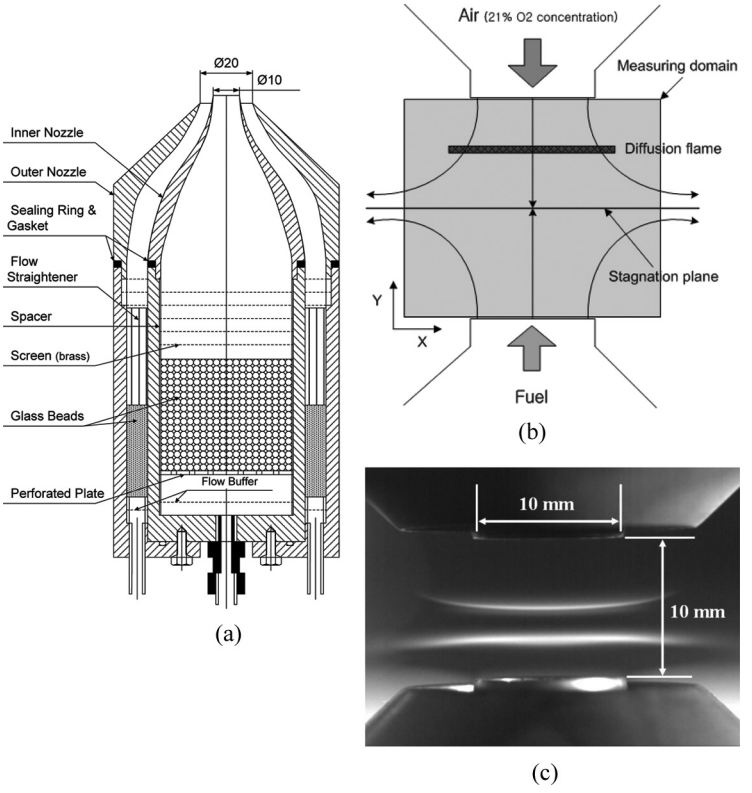

Figure 2 (a) Schematic of the burner [35], (b) estimation of flame structure and stagnation plane, and (c) direct photo of pure butane diffusion flame.

harmonic (532 nm) of a Nd:YAG laser (Continuum, PL 8000) was tuned to 283.01 nm to excite the $Q_1(6)$ OH transition of the 1–0 band $X^2\prod \Rightarrow A^2\sum^+$ system using a dye laser (Rhodamine 590) and frequency doubler. Excitation of the $Q_1(6)$

Table 3 Test conditions and measuring parameters

Test conditions	
Shielding gas (Ar, N_2)	1,000 sccm (0.04464 mol/min)
Air (21% O_2)	Nozzle exit velocity = 21.22 cm/sec
Mixed fuel(LPG + DME)	Fuel temperature = 25°C
Measurements	
1. Direct images	
2. Schlieren photography	
3. Flow characteristics (hot-wire anemometer)	
4. Distributions of OH radicals (laser-induced fluorescence)	
5. NOx emissions (NOx analyzer)	
6. Flame temperatures (R-type thermocouple)	

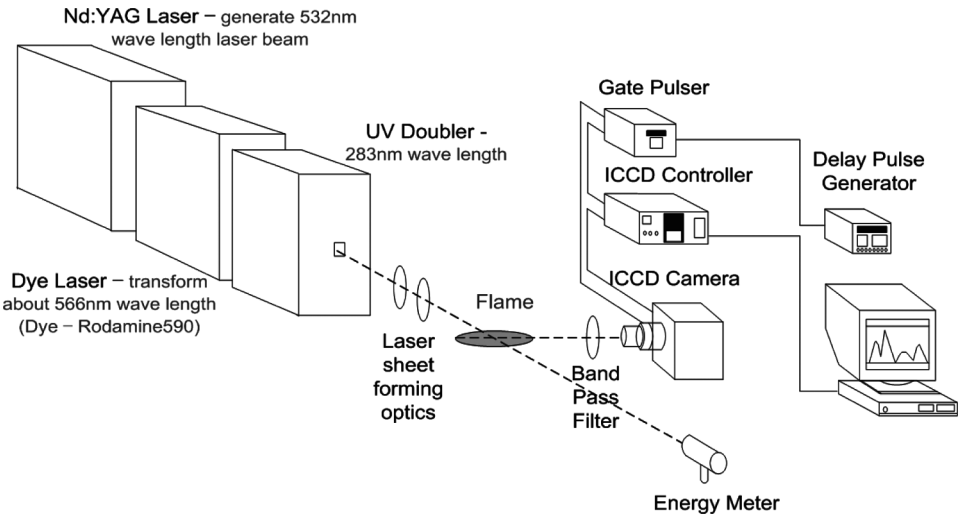

Figure 3 Schematic of PLIF system for OH-radical measurement.

OH transition was selected to minimize the temperature (1500–2000 K) sensitivity of this population within the absorbing level. The laser system provides 10 Hz pulses of about 10 ns in the 283-nm-wavelength range with a mean laser energy between 1.5 and 2.0 mJ/pulse. The OH fluorescence signal corresponded to the (1, 1) and (0, 0) transition bands between 305 and 320 nm.

Using cylindrical and spherical lenses, the laser beam was formed into a thin vertical sheet focused at the center of the burner. The OH LIF signal was captured by an intensified charge-coupled device (ICCD) camera (Princeton Instrument, PI-MAX) at right angles to a commercial UV transmitting camera lens (Nikon, $f = 105$ mm). To minimize noise, a combination of colored glass (Schott, low pass filter: WG305, and band pass filter: UG11) was used, and the gate time for the ICCD camera was set to 10 ns. Because an excited atom falls back into the ground state after a short period of time (typically 1–100 nsec), the programmable timing generator (PTG) of the laser system and the ICCD camera were synchronized using a pulse delay generator (DG535) that considered the laser travel time.

EXPERIMENTAL RESULTS AND DISCUSSION

Flow Measurement

In these experiments, the mass flow rates of the fuel and air were set to 1000 sccm using digital MFC (Brooks 5850E). To understand the fundamental combustion characteristics of the fuels, experiments were conducted at 1 atm and 25°C. Also, the flow velocities (u_{fuel} and u_{oxidizer} for fuel and air, respectively) were the same at the exit plane of the nozzle (22.12 cm/s) for all cases.

To verify flow stability, the velocity profile at the nozzle exit was measured by hot-wire anemometry with I-type hot-wire probes. Hot-wire probes were traversed at intervals of 0.5 mm using a 3-D traverse system with an accuracy of 0.01 mm over a

spanwise range of ±5 mm from the nozzle center. At each measurement point, velocity was measured at five instances and then averaged.

Global strain rates were calculated is $a = 102.7\,s^{-1}$ for butane, $a = 94.91\,s^{-1}$ for propane, and $a = 96.12\,s^{-1}$ for DME according to:

$$a = \frac{2(-u_O)}{L}\left[1 + \frac{u_F}{-u_O}\sqrt{\frac{\rho_F}{\rho_O}}\right], \tag{1}$$

where the velocity (u) subscripts F and O stand for the fuel and oxidizer, respectively; L is the distance between the nozzles (10 mm); and ρ is the gas density.

Figure 4a shows the velocity profile across the nozzle exit 4 mm from the nozzle tip at a mass flow rate of 1000 sccm; it is axisymmetric and uniform across the 2.5-mm radius perpendicular to the nozzle. Figure 4b demonstrates how the center-point axial velocity varies linearly with the mass flow rate.

Flame Structure

In these experiments, flame images were captured with a high-speed camera to visualize the flame structure. The distance between the camera and the burner was held constant in order to facilitate comparisons of the structures and stability of the flames for different DME fractions in the blend fuels.

Figure 5 compares the photos of flames that were stable and flat within the inner nozzle region. Outside that region, the flames lifted upward due to buoyancy. Varying the DME fraction did not affect the location of the stagnation plane; however, increasing DME concentrations made the flame shorter and thicker and moved it toward the upper oxidizing nozzle. Figure 5 also shows that the flame color changes with variation in DME fraction. For 100% butane, both a whitish pale-yellow flame (lower luminous zone) and a dark-blue flame (upper luminous zone) were observed. When the DME fraction was over 50 mole%, the lower pale-yellow flame disappeared. When the DME fraction increased to 100 mole%, the color and shape of

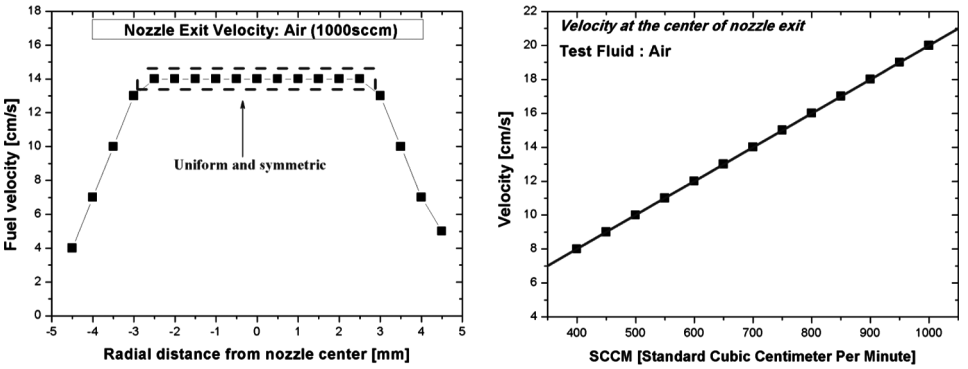

(a) (b)

Figure 4 (a) Velocity profile 4 mm from nozzle tip (single jet); and (b) nozzle exit velocities at various mass flow rates.

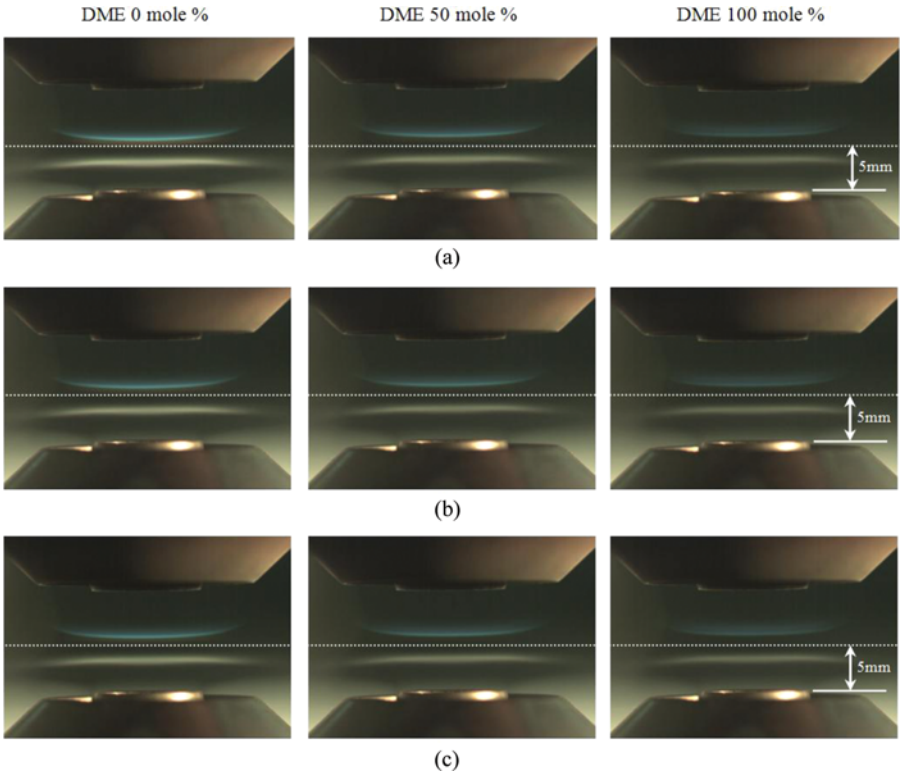

Figure 5 (a) Photos of butane 100%, (b) butane 80% + propane 20%, and (c) butane 75% + propane 25% with various DME fractions. (Figure is provided in color online.)

the flame changed from thin, luminous, dark-blue to thick, non-luminous, pale-blue. This indicates that the flame temperature increased with increasing DME fraction; given that color is a function of temperature, a blue flame represents hotter fields. Increasing flame temperature with increasing DME is due to the oxygen atoms in the DME (~35% by mass), which supply oxygen to the reaction zone similarly to that in premixing. Such oxygen premixing also made the flame thicker.

Despite the lower stoichiometric fuel/air ratio of the higher-oxygen-content DME compared to those of butane and propane, the flame thickness increased and moved toward the oxidizer nozzle with increasing DME fraction. The reaction zone also grew larger with DME fraction due to its fast pyrolysis. Arcoumanis et al. (2008) reported that C–O bonds break more easily than C–H bonds because of lower bond energy and distorted shape. At high temperatures, and because of low C–O bond energy, DME is prone to decomposition according to the following two free radical mechanisms (Curran et al., 1998):

$$CH_3OCH_3 \rightarrow CH_3O\ (31\,\mathrm{g/mol}) + CH_3\ (15\,\mathrm{g/mol}) \tag{2}$$

$$CH_3OCH_2 \rightarrow CH_3\ (15\,\mathrm{g/mol}) + CH_2O\ (30\,\mathrm{g/mol}) \tag{3}$$

The molecular weights of DME radicals are lower than those of other intermediate alkanes. Generally, light molecules have higher effusion rates. This means that the DME radicals more easily penetrate into and mix with the oxidizer stream.

Photos of the flame structures were captured using Schlieren photography. In gas flows with large temperature gradients, the Schlieren imaging technique is used to visualize high-temperature regions (i.e., the flame and its immediate surroundings). Figure 6 shows how the location and shape of the flame zone change with DME concentrations. For pure LPG, the flame region exhibits a more curved appearance due to the momentum of the constituents of the oxidizing fuels. These constituents are concentrated in a narrower reaction zone than those of DME. Because DME has a wider reaction zone, flame curvature decreases as DME concentration increases. Figure 6 also shows that the reaction zone expanded toward the upper oxidizer nozzle when DME concentration increased, which is consistent with the evidence shown in Figure 5.

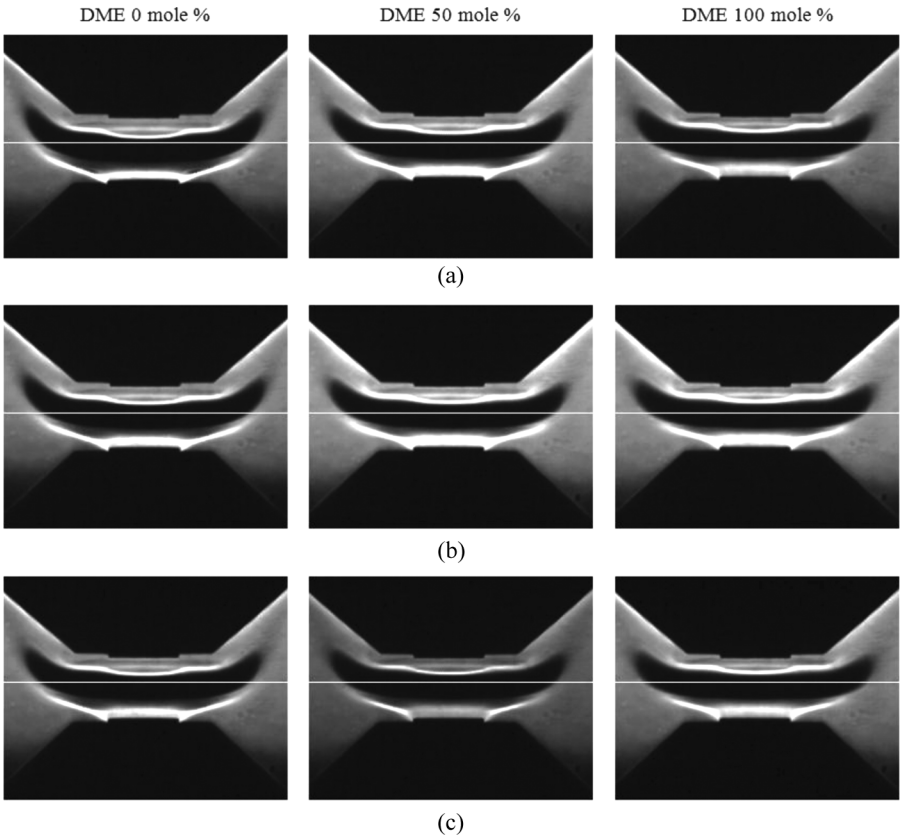

Figure 6 Schlieren photographs of flame location for (a) butane 100%, (b) butane 80% + propane 20%, and (c) butane 75% + propane 25% with various DME fractions.

Flame Temperature

An R-type thermocouple was made by spot-welding platinum and platinum–13% rhodium wire pairs, which were custom made by inserting the wires into a ceramic insulation tube inside a stainless tube. The junctions were nearly perfect spheres in which the diameters were consistently 1.2 mm with wire diameters of 0.15 mm. The thermocouple was not coated because catalytic effects were expected to be small in these nonpremixed flames. Flame temperatures along the centerline and in the radial direction were measured within ±5 K uncertainty.

The thermocouple was moved using a 3-D traverse system over the range ±7 mm with an accuracy of ± 0.01 mm uncertainty in the span-wise direction from the nozzle center and across a range of 0–10 mm in the streamwise direction from the lower nozzle. The thermocouple traversed the flame at 0.5 mm increments; outside the flame, the thermocouple was moved at 1-mm increments. At each measurement point, the flame temperature was measured five times and then averaged. Because the temperature distribution was axisymmetric, data were collected from the center (inside of the flame; high-temperature region) to the outside (radially outward; low-temperature region).

The signals produced by the thermocouple were sent to an A/D board and stored in a data-acquisition system programmed by LabVIEW. Because of heat loss due to radiation, the voltage produced by the thermocouple corresponded to a temperature that was lower than the true gas temperature. The difference between the measured and true gas temperature was calculated by equating the heat transferred to the thermocouple from the gas to that lost by radiation.

If conduction along the thermocouple wire and radiation to the junction are negligible, then this balance is (McEnally et al., 1997):

$$\varepsilon\sigma T_{\mathrm{m}}^4 = \left(\frac{k_{g0}\mathrm{Nu}}{2D}\right)\left(T_{\mathrm{real}}^2 - T_{\mathrm{m}}^2\right), \tag{4}$$

where ε is the junction-bead emissivity, σ is the Stefan–Boltzmann constant (i.e., $\sigma = 5.7 \times 10^{-8}\,\mathrm{W\,m^{-2}\,K^{-4}}$), T_{m} is measured temperature, D is the junction-bead diameter, and $k_{g0} = 6.54 \times 10^{-5}\,\mathrm{Wm^{-2}\,K^{-4}}$ is the gas thermal conductivity (McEnally et al., 1997). For a bead diameter of $D = 1.2$ mm and emissivity of platinum metal of Bradley and Entwistle (1961):

$$\varepsilon_{pt} = 9.6 \times 10^{-5} T + 0.056, \tag{5}$$

the Nusselt number is:

$$\mathrm{Nu} = \frac{hD}{k} = 2 + (0.4\mathrm{Re}^{0.5} + 0.06\mathrm{Re}^{0.667})\mathrm{Pr}^{0.4}, \tag{6}$$

where Re is the Reynolds number and Pr is the Prandtl number at the junction point of the thermocouple. Placing the thin wire normal to the low-Re gas flow ($0.02 < \mathrm{Re} < 44$) with nozzle exit velocities of fuel and air of ~0.2 m/s yielded $\mathrm{Nu} \approx 2$.

Figure 7 shows the increase of maximum flame temperature with DME fraction. For pure butane, the maximum temperature was 1674 K. For butane

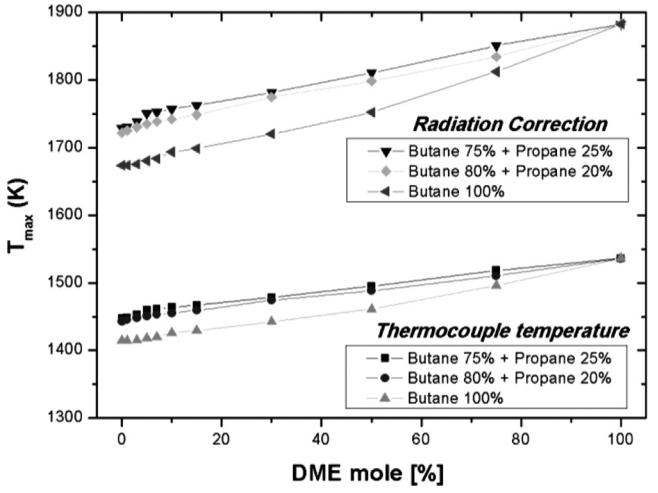

Figure 7 The variation of maximum temperature with various DME fractions.

80% + propane 20% (mass), the maximum temperature was 1722 K. For butane 75% + propane 25% (mass), the maximum temperature was 1729 K. For pure DME, the maximum temperature was 1883 K.

Because the low heating value (LHV) of propane is higher than that of butane, the maximum flame temperature increased with increasing propane content ratio, as shown in Table 1. However, the LHV of DME was the lowest on the list. Moreover, the adiabatic flame temperature of DME was the lowest; the adiabatic flame temperatures of butane, propane, and DME were 2240 K, 2250 K, and 2227 K, respectively. Despite the lowest LHV and adiabatic flame temperature of DME, the maximum flame temperature increased with increasing DME mole fraction in each type of LPG. This phenomenon can be explained by the fast pyrolysis (or reaction) of DME in the nonpremixed counterflow combustion system due to the C–O bond structure of DME. DME has the fastest maximum burning velocity as shown in Table 1. For example, the maximum fuel consumption rate of DME was two times greater than that of C_2H_6 despite identical atomic compositions (Kim et al., 2009). Apparently, DME burns faster and generates more heat per combustion time than propane and butane. Propane and butane are known to have stronger C–C bond structures. Also, there is less radiative heat loss to soot with increasing DME fraction, because the oxygen content of DME yields smokeless emissions (Fleisch et al., 1995; Kajitani et al., 1997). In this study, however, the faster fuel consumption rate was the primary reason for the elevated DME flame temperature because radiative losses are relatively minimal.

Figure 8a shows the flame temperature profiles of butane with various DME fractions, Figure 8b shows the temperature profiles of butane 80% + propane 20% with various of DME fractions, and Figure 8c shows the temperature profiles of butane 75% + propane 25% with various DME fractions. In the main flame region, the temperature distribution was symmetric and flat. As shown in Figures 5 and Figure 7b, an increase in DME concentration made the flame thicker and moved it closer to the upper nozzle.

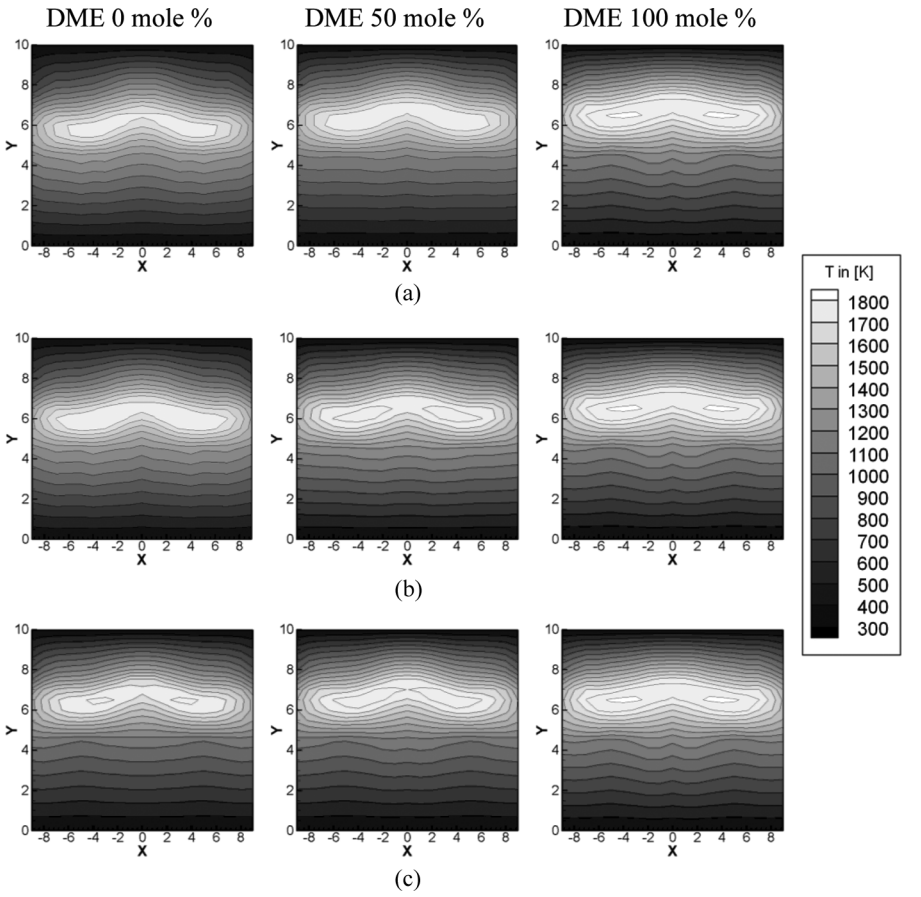

Figure 8 Flame temperature profiles for (a) butane 100%, (b) butane 80% + propane 20%, and (c) butane 75% + propane 25% with various DME fractions using an R-type thermocouple.

Emission Characteristic of NOx

The radial distribution of NOx concentrations was measured with a probe traversing the centerline. NOx was measured with a chemiluminescence photo diode detector (California Analytical, model CLD400). The calibration gas was a mixture of 100 ppm NO in N_2.

The probe moved across a range ± 15 mm in the spanwise direction from the nozzle center and from 0–10 mm in the streamwise direction from the lower nozzle. At each measurement point, NOx was measured five times and then averaged.

Figure 9a shows the NOx concentration profile for 100% butane at different axial (H; height from bottom burner) and radial locations from the lower nozzle center. NOx concentrations increase as the probe gets closer to the flame but decrease when the probe comes in contact with the flame. This occurred because the flame decreased in size and deformed as the probe approached.

Figure 9b shows the variation of maximum NOx concentration with DME concentration for different LPG types. The maximum NOx concentration decreased

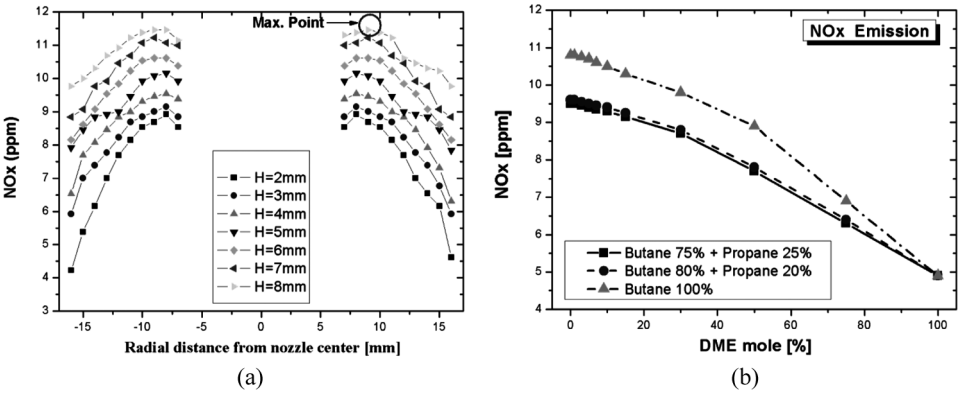

Figure 9 (a) NOx concentrations at various heights and (b) the variation of NOx emissions with DME fractions.

with increasing DME concentration for all LPG types. This is an interesting observation, considering that increasing DME concentrations also increased the maximum flame temperature (see again Figure 8).

According to Figure 9b, maximum NOx concentrations of DME flames were as much as 55% lower than those from pure butane. The maximum NOx concentration of a DME flame was as much as 48% lower than that of an LPG (butane 75% + propane 25%) flame. Clearly, DME combustion chemistry impacted NOx formation.

NOx was produced through both thermal and prompt NO mechanisms. The reburning mechanism of NOx was the primary path of destruction, and it occurred mostly through oxidation by intermediates such as C, CH_2, and HCCO generated during fuel pyrolysis and oxidation (Kim et al., 2009). Hwang et al. (2009) reported the removal of NOx in the fuel-rich region through the reburning reaction path:

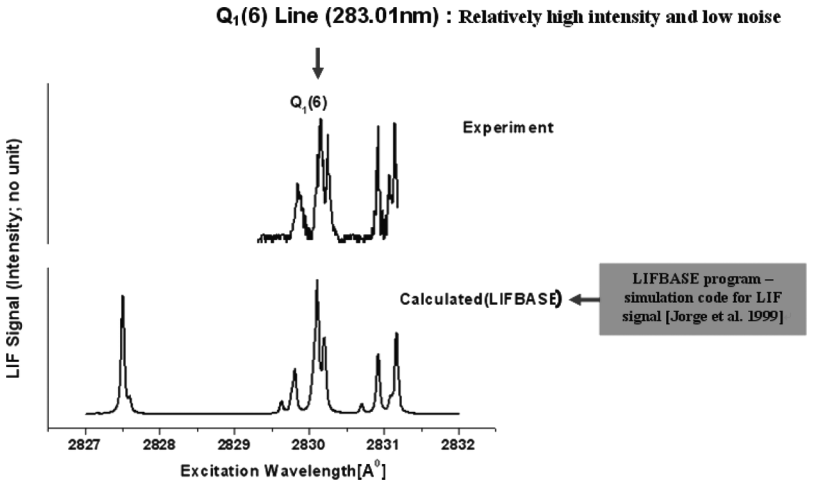

Figure 10 Comparison of excitation scan of OH with LIFBASE prediction at 1500 K and atmospheric pressure.

$NO + HCCO = HCNO + CO$. This phenomenon, however, was not apparent in the C_2H_6 flame. Instead, oxygen-containing radicals such as HCCO likely contributed to the NOx removal in DME flames. Thus, DME has reduced NOx emissions because of greater oxidation.

Distribution of OH Radicals

For a better understanding of DME and DME/LPG-blended fuel combustion characteristics, OH radical distributions in DME, LPG, and DME/LPG laminar diffusion flames were measured by planar laser induced fluorescence (PLIF).

The OH radical is a principal intermediate in combustion processes and can be used to identify the chemically reacting region of a flame. OH radicals are commonly produced through $H + O_2 = OH + O$ and $O + H_2 = H_2 + OH$ pathways. These OH

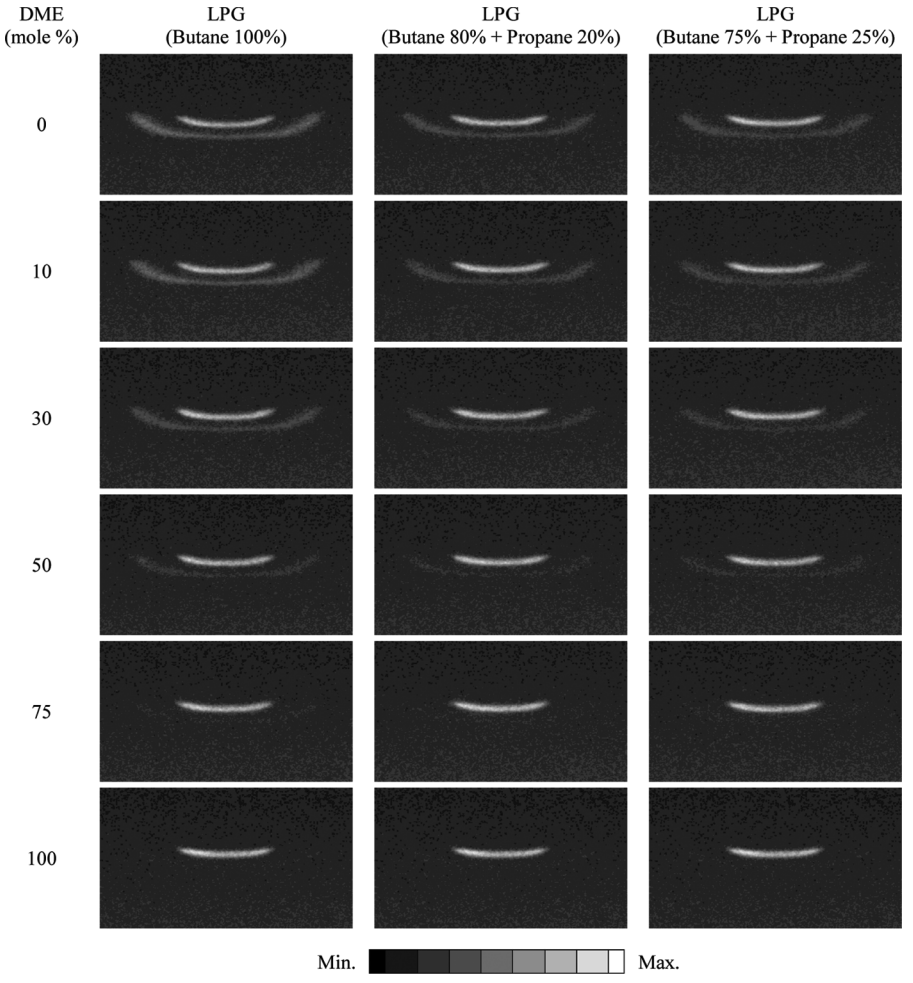

Figure 11 Two-dimensional OH-radical profiles at various DME fractions in LPG.

radicals initiate hydrocarbon oxidation by reacting with and removing the H atom from the fuel. In addition, OH radicals could be consumed in the CO oxidation reaction $OH + CO = CO_2 + H_2$. PLIF images show OH radical concentrations, and therefore, they outline the reaction zone in the flame.

Figure 10 shows an excitation scan along with the theoretical prediction using LIFBASE software (Luque and Crosley, 1999). An accurate, specific wavelength of fluorescence is required to obtain reliable OH signals, so the experimental data using various excitation wavelengths are compared with synthetic emission spectra generated by LIFBASE for pure butane ($T = 1500$ K) at atmospheric pressure. The emission spectra confirm that the signal recorded by the imaging camera is that of OH fluorescence.

Figure 11 shows planar images of OH-radical luminous intensities for various DME concentrations and LPG types. These images were made by superimposing two snapshots of the counterflow burner with the OH-radical signals using a fixed ICCD camera. As shown in Figure 11, there are two signal layers. The upper layer (stronger signal) shows OH radicals above the flame; the bottom layer (weaker signal) is the reflection of the soot. Despite the use of UG-11 and WG-305 glass filters, unwanted soot signals could not be removed completely. From top to bottom in the figure, the DME mole fraction varied from 0 to 1. The OH distributions for the various LPG blends exhibited a similar trend (compare columns in Figure 11), because OH radicals can be generated by various reaction paths and the fuel type is not a dominant factor (Curran et al., 1998). However, adding DME decreased soot signal below the flame as shown through the comparison of the rows in Figure 11. This is due to the high oxygen content of DME, which resulted in less soot generation in the fuel-rich region. Although adding DME decreases soot production, it has a nonlinear effect on OH concentrations. At first, adding DME decreases OH, but at 30% DME, OH shows increased concentrations. At higher DME levels, OH concentrations decrease, as is evident when comparing the rows in Figure 11.

CONCLUSIONS

Experimental studies were conducted to investigate flame structures, flame temperatures, concentrations of NOx, and OH radical characteristics of DME/LPG-blended fuel flames. Several conclusions are reported:

1. The counterflow flame grew wider, and its location moved closer to the oxidizer nozzle with increasing DME mole fraction. This shift toward the oxidizer nozzle can be explained by the fast pyrolysis of DME, whose molecular structure has a weak C–O bond. As a result, radicals such as CH_3, CH_2O, and CH_3O were more easily formed. The molecular weights of these radicals were lower than those of the intermediate radicals of butane and propane. Generally, lighter molecules contained higher effusion rates. This indicates that the decomposed radicals of DME more easily mix and penetrate into the oxidizer stream.
2. As the DME-to-propane ratio increased, the maximum flame temperature increased. Because the LHV and adiabatic flame temperature of propane were higher than those of butane, the maximum flame temperature increased with increasing propane mass fraction. Despite the lower LHV and adiabatic flame

temperature of DME, maximum flame temperatures increased with increasing DME mole fraction in each type of LPG because of the fast pyrolysis and oxidation of DME.

3. Despite flame temperature increases with increasing DME mole fraction, NOx concentrations decreased with increasing DME mole fraction for LPG mixtures. The formation and destruction characteristics of NO in the initial stage of DME oxidation were very different in comparison to those in butane and propane oxidation. Seemingly, the increase in oxygen-containing radicals such as HCCO from DME yield reduced NOx in the fuel-rich region.
4. Although DME produced OH radicals by various reaction paths, measured OH signals of the various fuel flames did not show distinct differences in the PLIF images. Thus, OH-radical profiles of the various LPG blends were similar. However, soot signals below the flame were also captured. These signals decreased as DME concentrations increased, indicating that DME generated less soot in the fuel rich region.

ACKNOWLEDGMENTS

This research was supported by the Energy & Resource Recycling Project of Korea Institute of Energy Technology Evaluation and Planning. This work was partly supported by a Korea University Grant (2011).

REFERENCES

Arcoumanis, C., Bae, C.S., Crookes, R., and Kinoshita, E. 2008. The potential dimethyl ether (DME) as an alternative fuel for compression-ignition engines: A review. *Fuel*, **87**, 1014–1030.

Bradley, D., and Entwistle, A.G. 1961. Determination of the emissivity, for total radiation, of small diameter platinum-10% rhodium wires in the temperature range 600–1450°C. *Br. J. Appl. Phys.*, **12**, 708–711.

Curran, H.J., Pitz, W.J., Westbrook, C.K., Dagaut, P., Boettner, J.-C., and Cathonnet, M. 1998. A wide range modeling study of dimethyl ether oxidation. *Int. J. Chem. Kinet.*, **30**(3), 229–241.

Fleisch, T., McCarthy, C., Basu, A., and Udovich, C. 1995. A new clean diesel technology: Demonstration of ULEV emissions on a Navistar diesel engine fueled with dimethyl ether. SAE paper 950061.

Hwang, C.H., Lee, C.E., and Lee, K.M. 2009. Fundamental studies of NOx emission characteristics in dimethyl ether (DME)/air non-premixed flames. *Energy Fuels*, **23**, 754–761.

Kajitani, S., Chen, Z.L., Konno, M., and Rhee, K.T. 1997. Engine performance and exhaust characteristics of direct-injection diesel engine operated with DME. SAE paper 972973.

Kim, T.H., Kim, J.M., Hwang, C.H., Kum, S.M., and Lee, C.E. 2009. The effect of chemical structure of dimethyl ether (DME) on Nox formation in nonpremixed counterflow flames. *J. Mech. Sci. Technol.*, **23**, 1885–1892.

Lee, M.C., Seo, S.B., Chung, J.H., Joo, Y.J., and Ahn, D.H. 2009. Industrial gas turbine combustion performance test of DME to use as an alternative fuel for power generation. *Fuel*, **88**, 657–662.

Lee, S.H., Oh, S.M., and Choi, Y. 2009. Performance and emission characteristics of an SI engine operated with DME blended LPG fuel. *Fuel*, **88**, 1009–1015.

Luque, J., and Crosley, D.R. 1999. LIFBASE: Database and spectral simulation program (v. 2.0). SRI International Report MP 99-009.

Marchionna, M., Patrini, R., Sanfilippo, D., and Miliavacca, G. 2008. Fundamental investigations on dimethyl ether (DME) as LPG substitute or make-up for domestic uses. *Fuel Proc. Technol.*, **89**, 1255–1261.

McEnally, C.S., Koylu, Ü.O., Pfefferle, L.D., and Rosner, D.E. 1997. Soot volume fraction and temperature measurements in laminar nonpremixed flames using thermocouples. *Combust. Flame*, **109**, 701–720.

Morsy, M.H., and Chung, S.H. 2007. Effect of additives on ignition of methane at homogeneous charge compression ignition engine-like conditions. *Proc. Inst. Mech. Eng., Part D.: Automobile Eng.*, **221**, 605–619.

Ohno, Y., Ogawa, T., Shikada, T., and Inoue, N. 2000. DME production technology and operation results of 5 tons/day plant. *Proceedings of the International DME Workshop*, University of Tokyo, September 7, Japan DME Forum, pp. 73–81.

Semelsberger, T., Borup, R., and Greene, H. 2006. Dimethyl ether (DME) as an alternative fuel. *J. Power Sources*, **156**, 497–511.

Song, K.H., Nag, P., Litzinger, T.A., and Haworth, D.C. 2003. Effects of oxygenated additives on aromatic species in fuel-rich, premixed ethane combustion: A modeling study. *Combust. Flame*, **135**, 341–349.

Ying, W., Longbao, Z., and Hewu, W. 2006. Diesel emission improvements by the use of oxygenated DME/diesel blend fuels. *Atmos. Environ.*, **40**, 2313–2320.

Yoon, S.S., Anh, D.H., and Chung, S.H. 2008. Synergistic effect of mixing dimethyl ether with methane, ethane, propane, and ethylene fuels on polycyclic aromatic hydrocarbon and soot formation. *Combust. Flame*, **154**, 368–377.

Zhang, B., Fu, W., and Gong, J. 2006. Study of fuel consumption when introducing DME or ethanol into diesel engine. *Fuel*, **85**, 778–782.